INTELLIGENT DECOUPLING CONTROL SYSTEM OF COMPLEX INDUSTRIAL PROCESS AND APPLICATION

Tianyou Chai, Heng Yue, and Lianfei Zhai

Research Center of Automation, Northeastern University,
Shenyang, 110004, P. R. China, Email: tychai@mail.neu.edu.cn

Abstract: A new decoupling control structure is presented for complex industrial processes, which consists of a feedback controller, a decoupling compensator and a feedforward compensator for unmodeled dynamics. Using this structure, an intelligent decoupling control system is established which realizes an adaptive decoupling control strategy for industrial processes with integrated complexities by using a neural network plus a switching mechanism. Such system can be easily implemented on distributed control systems (DCS) and has been successfully applied to ball mill pulverizing systems for 200MW power units. Simulation and industrial application show its robust performance of the proposed system and its potential prospect in the industry. *Copyright © 2005 IFAC*

Keywords: Control applications; Multivariable control systems; Decoupling problems; Intelligent control; Switches; Neural networks; Distributed control systems

1. INTRODUCTION

Nowadays heavily coupled control loops are seen in many complex industrial processes. These coupling effects often result in undesired performance for control systems. As such, it is important to investigate the realization of decoupling control, a topic that has received an increased attention in control engineering practice. Indeed, decoupling control was initially developed for deterministic linear systems (Shinskey, 1979). For linear systems with unknown parameters, many adaptive decoupling control algorithms have been proposed. For example, multivariable adaptive decoupling controllers were presented by McDermott and Mellichamp (1986), and Lang, *et al*. (1986), which combined the decoupling design with a self-tuning control structure. Also, pole placement adaptive decoupling control algorithm was developed by Wittenmark, *et al*. (1987). In these approaches, the coupling effects among control loops were viewed as measurable disturbances so that they can be eliminated through a feedforward compensator (Chai, 1990). To deal with coupling in nonlinear systems, neural networks and fuzzy methods have been adopted. Relevant approaches can also be found in Wu and Chai (1995)

and Zhu, *et al*. (1999). These decoupling control methods not only require accurate mathematic models of the controlled processes, but also are difficult to be implemented in DCS.

In recent years, DCS have become more and more popular in industrial process control because of their high reliability. In practice, control engineers divide multivariable industrial processes into many SISO systems without considering the coupling effects among each loop so as to use the standard control module software of DCS to realize the required control tasks. If the coupling effects are very strong, they would generally result in bad performance of the control systems or even lead to an unstable operation. Therefore, it is very important to develop effective decoupling controllers that are applicable in DCS.

In this paper, an intelligent decoupling control approach is developed for the control of real industrial processes with integrated complexities (e.g. strong coupling, serious nonlinearity, and dynamics without accurate mathematics model). The proposed approach uses the generalized minimum variance control based decoupling design, which was initially proposed for unknown linear systems (Chai, 1990)

and later extended to nonlinear systems (Chai, 2005), and a multiple models method (Chen and Narendra, 2001). The intelligent decoupling control system for complex industrial processes is applied to a ball mill pulverizing system of 200MW power unit.

2. STRUCTURE OF NONLINEAR DECOUPLING CONTROL SYSTEM

2.1 Statement of the problem

In practical industrial processes, control systems operate in a neighbourhood of several operating points. There are possibly multiple operating points which are known and determined by various production indices. Sometimes, the changes of operating points will cause the variations of parameters as well as possible structural changes of their dynamics. As a result, around its ith operating point, the complex industrial process to be controlled can be generally described by

$$y(t+1) = f_i[y(t),\cdots,y(t-n_a+1),u(t),\cdots,u(t-n_b)],$$
$$i = 1,\cdots,m \quad (1)$$

where $y = [y_1,\cdots,y_k]^T \in R^k$ and $u = [u_1,\cdots,u_k]^T \in R^k$ are system output and input vectors, respectively; n_a and n_b are system orders; m represents the number of multiple operating points; $f_i(\cdot) = [f_{i1}(\cdot),\cdots,f_{ik}(\cdot)]^T$ is a vector-valued nonlinear function that is assumed unknown and continuously differentiable. To simplify the notations, operating point number i is omitted. Equation (1) can be divided into an approximated linear model (with lower order) for the controller design plus a higher order nonlinear term as expressed in the following:

$$y(t+1) = -\overline{A}(z^{-1})y(t) + B(z^{-1})u(t)$$
$$+ v[y(t),\cdots,y(t-n_a+1),u(t),\cdots,u(t-n_b)]$$
$$= -\overline{A}(z^{-1})y(t) + \overline{B}(z^{-1})u(t) + \overline{\overline{B}}(z^{-1})u(t) \quad (2)$$
$$+ v[y(t),\cdots,y(t-n_a+1),u(t),\cdots,u(t-n_b)]$$
$$= \Theta \cdot x^T(t) + v[x(t)]$$

where $\overline{A}$, $\overline{B}$ and $\overline{\overline{B}}$ are polynomial matrices in terms of the unit back shift operator z^{-1} with $\overline{A}$ and $\overline{B}$ being diagonal (Introduce $A = I + z^{-1}\overline{A}$.), and $\overline{\overline{B}}$ is a polynomial matrix with zero diagonal elements, and

$$x(t) = [-y^T(t),\cdots,-y^T(t-n_a+1);u^T(t),\cdots,u^T(t-n_b);u^T(t),\cdots,u^T(t-n_b)]$$
$$\Theta = [A_1,\cdots,A_{n_a};\overline{B}_0,\cdots,\overline{B}_{n_b};\overline{\overline{B}}_0,\cdots,\overline{\overline{B}}_{n_b}]$$

whilst the elements are coefficients matrices of A, $\overline{B}$ and $\overline{\overline{B}}$. The nonlinear term represents the unmodeled dynamics of the following format

$$v[x(t)] = y(t+1) + \overline{A}y(t) - \overline{B}u(t) - \overline{\overline{B}}u(t)$$
$$= f(\cdot) + \overline{A}y(t) - \overline{B}u(t) - \overline{\overline{B}}u(t) \quad (3)$$

Qualitatively, the purpose of decoupling control is to determine an input control law so that all the signals in the closed loop system remain bounded, whilst the output vector y is confined in some pre-specified range, and the influence of the couples is suppressed as small as possible.

2.2 Structure of decoupling control system

As shown in Fig.1, the structure of the decoupling control system is proposed by combining a feedback controller, a decoupling compensator and a feedforward compensator for $v[x(t)]$.

The feedback controller, which is denoted by three diagonal polynomial matrices, namely $\overline{H}$, $\overline{R}$ and $\overline{G}$, is used to make sure that $y(t)$ can follow the reference input vector $w(t)$. The decoupling compensator $\overline{\overline{H}}$, which is a polynomial matrix with zero diagonal elements, is designed to decouple control loops. The feedforward compensator $\overline{K}$, which is a diagonal polynomial matrix, is employed to eliminate the influence of unmodeled dynamics $v[x(t)]$ to the closed loop system. Indeed, $v[x(t)]$ can be estimated by a neural network which is to be discussed in the following section. From Fig. 1, the control input can be calculated from

$$u(t) = \overline{H}^{-1}\{\overline{R}w(t) - \overline{G}y(t) - \overline{\overline{H}}u(t) - \overline{K}v[x(t)]\} \quad (4)$$

Substituting (4) into (2) yields

$$(\overline{H}A + z^{-1}\overline{B}\overline{G})y(t+1)$$
$$= \overline{B}\,\overline{R}w(t) + (\overline{H}\overline{\overline{B}} - \overline{B}\overline{\overline{H}})u(t) + (\overline{H} - \overline{B}\overline{K})v[x(t)] \quad (5)$$

From (5), it can be seen that $(\overline{H}A + z^{-1}\overline{B}\overline{G})$, $\overline{B}\overline{R}$ and $(\overline{H} - \overline{B}\overline{K})$ are diagonal matrices whilst matrix $(\overline{H}\overline{\overline{B}} - \overline{B}\overline{\overline{H}})$ has zero diagonal elements. Moreover, $\overline{H}$, $\overline{G}$ and $\overline{R}$ can be properly selected which can realize a unity gain for the steady channel gain from $w(t)$ to $y(t)$. Also, an appropriate choice of $\overline{\overline{H}}$ would suppress the influence of $(\overline{H}\overline{\overline{B}} - \overline{B}\overline{\overline{H}})u(t)$ to the lowest possible level. The effect of $(\overline{H} - \overline{B}\overline{K})v[x(t)]$ can be eliminated through an adequate choice of $\overline{K}$. For example, $\overline{H}$, $\overline{G}$, $\overline{R}$, $\overline{\overline{H}}$ and $\overline{K}$ can be chosen by combining the proposed structure with well-known control strategies such as predictive control, PID, generalized minimum variance control, etc. In specific, generalized minimum variance control strategy is discussed in the following.

The significance of the structure of such a decoupling control system can be seen from the expression of controller of every single loop

$$u_l(t) = (1/h_{ll}) \cdot \{r_{ll}w_l(t) - g_{ll}y_l(t) - [h_{l1}u_1(t) + \cdots + h_{l(l-1)}u_{l-1}(t) + h_{l(l+1)}u_{l+1}(t) + \cdots + h_{lk}u_k(t)] - k_{ll}v_l(t)\} \quad (6)$$
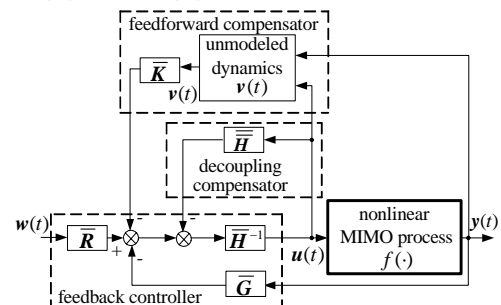

Fig. 1. Structure of decoupling control system

where r_{lj}, g_{lj}, k_{lj} and h_{lj} are the elements in the lth row and the jth column of $\overline{R}$, $\overline{G}$, $\overline{K}$ and H, with $H = \overline{H} + \overline{\overline{H}}$. From (6), it is known that the lth control input $u_l(t)$ only relies on the output $y_l(t)$, reference input $w_l(t)$, unmodeled dynamics $v_l[x(t)]$ of the lth control loop and other control inputs $u_1(t), \cdots u_{l-1}(t)$, $u_{l+1}(t), \cdots u_k(t)$. Since other control inputs and the estimation of $v[x(t)]$ can be easily obtained, it can be effectively implemented on DCS using standard control modules. When the compensating terms of decoupling and suppressing for unmodeled dynamics are not used, this control law becomes a conventional controller.

3. INTELLIGENT DECOUPLING CONTROL USING MULTIPLE MODELS AND NEURAL NETWORK

In this section, an intelligent decoupling control using multiple models and neural network is developed based on the above presented structure of decoupling control system for complex industrial processes.

3.1 Nonlinear decoupling controller

In order to choose $\overline{R}$, $\overline{G}$, $\overline{K}$ and H in (4), the following performance index (Chai, 2005) is introduced:

$$J = \left\| Py(t+1) - Rw(t) + Qu(t) + Su(t) + Kv[x(t)] \right\|^2 \quad (7)$$

where P, Q, R and K are the diagonal weighting polynomial matrices, S is a weighting polynomial matrix with zero diagonal elements. By solving the Diophantine equation as

$$P = FA + z^{-1}G \quad (8)$$

both F and G can be solved to give diagonal polynomial matrices structure. At this stage, one can choose $\overline{H}$, $\overline{\overline{H}}$, $\overline{R}$, $\overline{G}$ and $\overline{K}$ in (4) so as to satisfy $\overline{H} = F\overline{B} + Q$, $\overline{R} = R$, $\overline{G} = G$, $\overline{\overline{H}} = F\overline{\overline{B}} + S$ and $\overline{K} = F + K$. It can be proved that the optimal controller that minimizes (7) is described by

$$
\begin{aligned}
&[F\overline{B} + Q]u(t) \\
&= Rw(t) - Gy(t) - [F\overline{\overline{B}} + S]u(t) - [F + K]v[x(t)]
\end{aligned} \quad (9)
$$

Equation (5) can be written to read:

$$
\begin{aligned}
&[P\overline{B} + QA]y(t+1) \\
&= \overline{B}Rw(t) + [Q\overline{\overline{B}} - \overline{B}S]u(t) + [Q - \overline{B}K]v[x(t)]
\end{aligned} \quad (10)
$$

If the unmodeled dynamics is small, the control law can be calculated from

$$(F\overline{B} + Q)u(t) = Rw(t) - Gy(t) - (F\overline{\overline{B}} + S)u(t) \quad (11)$$

It can be seen that if P, Q, R, K and S are chosen as follows:

$$P\overline{B} + QA = \overline{B}R \quad (12)$$

$$Q\overline{\overline{B}} = \overline{B}S \quad (13)$$

$$Q = \overline{B}K \quad (14)$$

$$\left| PB + A(Q+S) \right| \neq 0 \quad |z| > 1 \quad (15)$$

then the closed loop system will be stable with a decoupling control effect and the tracking errors can be eliminated.

3.2 Estimation of unmodeled dynamics and models

As for the unmodeled dynamics $v[x(t)]$, a neural network is employed to perform an online estimation. It has $k(m+n+1)$ inputs and k outputs

$$\hat{v}[x(t)] = NN[x(t)] \quad (16)$$

where NN denotes the format of the neural networks, and $x(t)$ is the input vector. At the ith operating point, the recursive least square (RLS) algorithm is used to estimate the parameters of the model (2). The estimation of Θ_i is denoted by $\hat{\Theta}_i(t)$, and the linear estimation model M_{1i} is described by equation

$$M_{1i}: \hat{y}_{1i}(t+1) = \hat{\Theta}_i(t) \cdot x^T(t), \quad i = 1,2,\cdots,m \quad (17)$$

The neural network estimation model M_{2i} can be expressed by the following equation

$$M_{2i}: \hat{y}_{2i}(t+1) = \hat{\Theta}_i(t) \cdot x^T(t) + \hat{v}_i(t), \quad i = 1,2,\cdots,m \quad (18)$$

3.3 The switching system

A set of linear decoupling controllers $C_{11},\cdots,C_{1m}$ are designed for all linear models $M_{11},\cdots,M_{1m}$, whilst a set of nonlinear decoupling controllers $C_{21},\cdots,C_{2m}$ are obtained for all nonlinear models $M_{21},\cdots,M_{2m}$. In most industrial processes, the unmodeled dynamics $v[x(t)]$ is bounded and such an upper bound is known, (i.e. $\|v[x(t)]\| \le \Delta$), with a known upper bound for Δ. A performance criterion $J_{ji}(t)$ (Chen and Narendra, 2001) for model M_{ji} is defined as

$$J_{ji}(t) = \sum_{l=1}^{t} \frac{a_{ji}(l)[\|e_{ji}(l)\|^2 - 4\Delta^2]}{1 + \|x(l-1)\|^2} + c \cdot \sum_{l=t-N+1}^{t} [1 - a_{ji}(l)]\|e_{ji}(l)\|^2$$

$$j = 1,2 \text{ and } i = 1,\cdots,m \quad (19)$$

where $j = 1$ stands for linear, $j = 2$ denotes nonlinear,

$$a_{ji}(t) = \begin{cases} 1 & if \|e_{ji}(t)\| > 2\Delta \\ 0 & otherwise \end{cases}$$, N is an integer and $c \ge 0$

is a pre-specified constant, $e_{ji}(t) = y(t) - \hat{y}_{ji}(t)$ is the error vector between the system output $y(t)$ and the predicted output $\hat{y}_{ji}(t)$ which is produced by M_{ji}. At each time instant t, if model M_{ji} produces the smallest
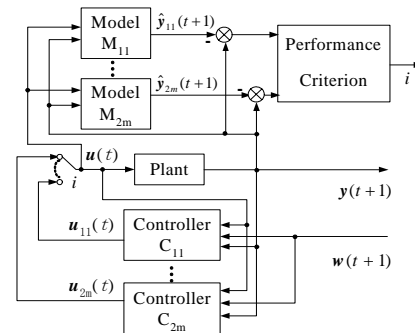

Fig. 3. Switching system

performance criterion $J_{ji}(t)$, then its associated certainty equivalence control input $u_{ji}(t)$ can be applied to the system by setting $u(t) = u_{ji}(t)$.

3.4 Intelligent decoupling control algorithm

The new intelligent decoupling control algorithm is divided into two parts: 1) offline controller design, and 2) adaptive compensating algorithm for the unmodeled dynamics and a switching mechanism. Through the offline controller design, a set of linear estimation model $M_{11}, \cdots, M_{1m}$ are identified by using the RLS algorithm. The related nonlinear estimation models $M_{21}, \cdots, M_{2m}$ are then established by using neural networks. Using these models, the corresponding controllers can be designed through (12)-(15), where a series of neural networks are established to approximate the unmodeled dynamics and trained in batch. The main tasks of the adaptive compensating algorithm for the unmodeled dynamics and the switching unit consist of 1) calculating the predicted outputs $\hat{y}_{ji}(t+1)$, 2) evaluating $J_{ji}(t)$, and 3) producing the smallest $J_{ji}(t)$ so as to select the model that links with the smallest $J_{ji}(t)$ as the model for the controller design.

Suppose that the unmodeled dynamics $v[x(t)]$ is globally bounded, and then it can be proved that the intelligent decoupling control ensures the uniform boundness of all the signals. Since the neural networks are regarded as universal approximators (Funahashi, 1989), the modelling error $\left\| v[x(t)] - \hat{v}(t) \right\|$ can be made less than any specified ζ over a compact set by properly choosing their structures and parameters. This means that if the modelling error converges to zero, the closed loop tracking error can be eliminated.

4. SIMULATION

To illustrate the effectiveness of the proposed decoupling control system, a simulation study is described in this section. The simulation is carried out from $t = 1$ to $t = 350$. When $t = 70$, the process to be controlled switches from Σ_1 to Σ_2 ; when $t = 220$, it switches from Σ_2 to Σ_3 where Σ_1 is described by

$$
\begin{aligned}
y_1(t+1) &= 0.4\sin[y_1(t)]/[0.5 + y_2(t-1)] \\
&\quad - 0.45 y_1(t-1) + 1.1u_1(t) + 0.8u_2(t)
\end{aligned}
\tag{20}
$$

$$
\begin{aligned}
y_2(t+1) &= \cos[y_2^2(t)] - 0.3 y_2(t-1) + 1.25u_2(t) \\
&\quad + 0.29\cos[u_1^2(t)] + 0.1u_2(t-1) + 0.32u_1(t-1)
\end{aligned}
\tag{21}
$$

and Σ_2 is described by

$$
\begin{aligned}
y_1(t+1) &= 0.6\sin[y_1(t)]/[0.6 + y_2(t-1)] \\
&\quad - 0.41 y_1(t-1) + 1.3u_1(t) + 0.5u_2(t)
\end{aligned}
\tag{22}
$$

$$
\begin{aligned}
y_2(t+1) &= \cos[y_2^2(t)] - 0.5 y_2(t-1) + 1.5u_2(t) \\
&\quad + 0.4545\cos[u_1^2(t)] + 0.3u_2(t-1) + 0.2u_1(t-1)
\end{aligned}
\tag{23}
$$

whilst Σ_3 is expressed by

$$
\begin{aligned}
y_1(t+1) &= 0.4\sin[y_1(t)]/[0.5 + y_2(t-1)] \\
&\quad - 0.45\sin(y_1(t-1)) + 1.1u_1(t) + 0.8u_2(t)
\end{aligned}
\tag{24}
$$

$$
\begin{aligned}
y_2(t+1) &= \sin[y_2(t)] - 0.3\sin[y_2(t-1)] + 0.3763 y_2(t-1) \\
&\quad + 1.25u_2(t) + 0.29u_1(t) + 0.1u_2(t-1) + 0.32u_1(t-1)
\end{aligned}
\tag{25}
$$

Three BP neural networks of the same structure are used, where only one hidden layer is employed with 20 nodes. $J_i(t)$ is defined by selecting $\Delta = 0.2$, $N = 3$ and $c = 1$. The following models are constructed and used in the control of the plant: a linear model of Σ_1 , as denoted by M_0 ; three nonlinear models as denoted by M_1, M_2, M_3 respectively. The reference inputs are given by $w_1(t) = 0.2 sign[\sin(\pi t/50)]$, $w_2(t) = 0.5$, respectively. The closed loop responses are shown in Fig. 4 and the corresponding control inputs are displayed in Fig. 5. It can be seen that a perfect tracking has been realized with a very small coupling effect. In addition, switching occurs mostly between M_1 and M_2 when the process is evaluated at Σ_2 , and between M_2 and M_3 when the process is based on Σ_3 .

5. APPLICATION IN BALL MILL PULVERIZING SYSTEMS

The proposed intelligent decoupling control system has been applied in ball mill coal-pulverizing systems of 200 MW units in a power plant.
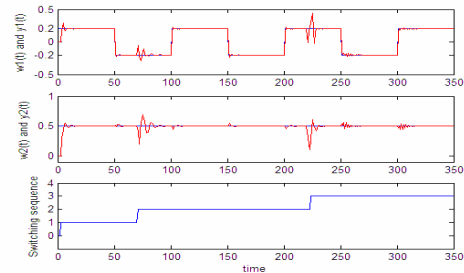

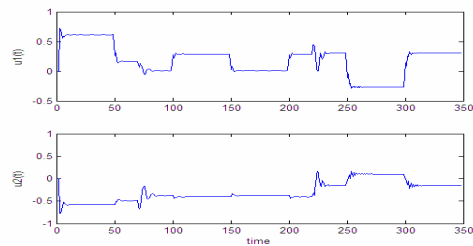Fig. 4. The performance of the switching system and switching sequence

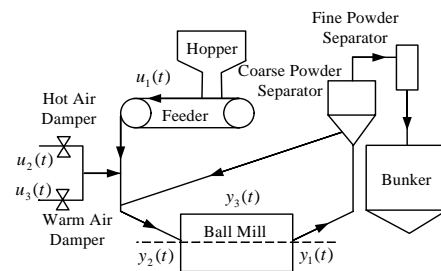Fig. 5. Corresponding control inputs $u_1(t)$ and $u_2(t)$

Fig. 6. Flow chart of ball mill pulverizing system

5.1 Process description

Ball mill pulverizing systems are important heat-power equipments in power plants. They are widely used at 200MW power units in China, where thousands of such power generation systems are installed. Ball mill pulverizing systems are used to pulverize raw coal into fine powder and then dry them so that coal powder can be sent into the boilers for burning. The flow chart of ball mill pulverizing system is shown in Fig. 6. The raw coal is sent from hopper to ball mill by coal feeder. In the ball mill, it is pulverized to fine powder by knocking and grinding of iron ball when the ball mill rotates. At the same time, the coal powder is dried and brought out of the ball mill by drying air, which is produced through a mixture of hot air and warm air by adjusting the hot air and warm air damper position. Then it is sent into the separator, where the coarse powder and fine powder are separated. Coarse powder is returned into the ball mill for regrinding and fine powder is sent into the bunker and then to boiler for burning.

Since this system has integrated complexities such as strong coupling, serious nonlinearity, large time delay, big variation of boundary condition, the conventional SISO control system cannot be used automatically. As such, the ball mill pulverizing system relies on human operations, leading to various accidents such as mill-blockage, over-temperature and mis-emission of pulverized coal powder. To prevent accidents, human operators are employed to control this system at an uneconomical operating point where a large volume of energy has been wasted. It has therefore become important yet difficult issue on how to realize decoupling control of such systems in China.

A nonlinear dynamic first principle model is established, which consists of the energy balance equation in the ball mill as follows:

$$
\begin{aligned}
&d\,[(C_{gq} W_{gq} + C_m W_m)T_m]/dt \\
&= C_{gz} G_{gz} T_{gz} + C_{lk} G_{lf} T_{lk} + B_{gm} C_{gm} T_c / 3.6 + Q_0 \\
&- C_m B_m T_m / 3.6 - C_{tf} (G_{gz} + G_{lf})T_m - Q_c
\end{aligned} \quad (26)
$$

and the mass balance equation of the form:

$$
\frac{dW_m}{dt} = \frac{B_{gm} - B_m}{3.6} \quad (27)
$$

Moreover, the equation of the inlet pressure P_{in} is given by:

$$
\frac{dP_{in}}{dt} = \frac{RT}{V_1}(G_{gz} + G_{lf} + \frac{B_{gm} \Delta W}{3.6} - \sqrt{\frac{P_{in} - \Delta P + P_0}{R_1}}) \quad (28)
$$

with

$$
\frac{d\Delta P}{dt} = 3(1 + 0.8\mu)\frac{\omega_{thr}^2}{2V_1}(G_i - G_o) \quad (29)
$$

$$
G_r = \sqrt{\frac{\Delta P_r K_r^2}{f_r (273 + T_r)}} \quad (30)
$$

$$
G_w = \sqrt{\frac{\Delta P_w K_w^2}{f_w (273 + T_w)}} \quad (31)
$$

being used as the physical models for the differential pressure ΔP, the hot-air and warm-air mass flow rates. The coal feeding rate is given by:

$$
B_{gm} = B_{g\max} K_{gm} \quad (32)
$$

where, K_{gm}, K_r, K_w and T_m are the feeder speed, the hot air damper position, the warm air damper position and the temperature of the mill outlet, respectively. The meanings of other variables can be found from the work by Chai, *et al.* (1999) and Tao, *et al.* (2004). Define the input variables as $u_1(t) = K_{gm}(t)$, $u_2(t) = K_r(t)$, $u_3(t) = K_w(t)$, and the output variables as $y_1(t) = T_m(t)$, $y_2(t) = P_{in}(t)$, $y_3(t) = \Delta P(t)$.

5.2 Decoupling control system and application

From the analysis of the process dynamics and the industrial experiments, the process model can be described by the following equations.

$$
A_{11} y_1(t+1) = B_{11} u_1(t) + B_{12} u_2(t) + B_{13} u_3(t) + v_1(t) \quad (33)
$$

$$
A_{22} y_2(t+1) = B_{21} u_1(t) + B_{22} u_2(t) + B_{23} u_3(t) + v_2(t) \quad (34)
$$

$$
A_{33} y_3(t+1) = B_{31} u_1(t) + B_{32} u_2(t) + B_{33} u_3(t) + v_3(t) \quad (35)
$$

where the orders of A and B are set to 2 and 1, respectively. Then the proposed decoupling control system strategy is used. To estimate the unmodeled dynamics (i.e., $v_1(t)$, $v_2(t)$ and $v_3(t)$), three BP neural networks are adopted, which have the same structure of 1 hidden layer and 20 hidden neurons. Matrices P, Q, R, S and K have been chosen as follows:

$$
P = R = I \ , \ Q = diag[\lambda_1,\lambda_2,\lambda_3] \cdot (1 - z^{-1}),
$$

$$
K = diag[k_1,k_2,k_3] \cdot (1 - z^{-1}), \ S = \begin{bmatrix} 0 & s_{12} & s_{13} \\ s_{21} & 0 & s_{23} \\ s_{31} & s_{32} & 0 \end{bmatrix} \cdot (1 - z^{-1})
$$

where the cut-and-try method is used.

To illustrate the effectiveness of the feedforward compensation for the unmodeled dynamics $v[x(t)]$, a comparative experiment between the proposed controller and a controller without the feedforward compensator is performed, where the warm air is taken as a disturbance and the responses of the other loops are reviewed. When the control system operates in a steady state, the warm air damper position u_3 is increased by 10% (i.e., by shifting the damper under a temporary manual control) so as to introduce the
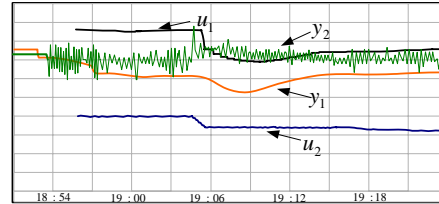

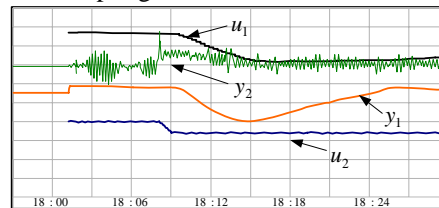Fig. 8. Experiment result of proposed intelligent decoupling controller

Fig. 9. Experiment result of the controller without feedforward compensator

warm air disturbance. Fig. 8 and Fig. 9 show the experiment results of the disturbance attenuation, from where it can be clearly seen that the outlet temperature y_1 and the inlet pressure y_2 can return to their original setpoints. The measurement ranges of the four variables (i.e., the outlet temperature y_1, the inlet pressure y_2, the feeder speed u_1 and the hot air damper position u_2) are 60°C~80°C of 2°C/grid, -1.0kpa~0.0kpa of 0.1kPa/grid and 0~100% of 10%/grid, respectively. The time scale is 3 minutes per grid. It can be seen from the experiment results that the fluctuations of the outlet temperature are within 2°C and the transient response time is about 6 minutes when the intelligent decoupling control is adopted. Moreover, the fluctuation of the outlet temperature y_1 is about 4°C and the transient response time is more than 15 minutes when the controller without the feedforward compensator is used. Apparently, the performance of the closed loop control system has been remarkably improved through the feedforward compensator.

The proposed decoupling control system has also been applied in the real process. The results are shown in Fig. 10. A comparison of the intelligent decoupling control with the existing manual control is shown in Fig.11. Under the decoupling control strategy, the outlet temperature y_1 can be kept within ± 3°C and the differential pressure y_3 is made within ± 0.1kPa. The average of the feeder speed u_1 can be realized as high as 90.5%. However, under the manual control the outlet temperature y_1 can only be constrained within ± 7°C and the differential pressure y_3 is within ± 0.3kPa, where the average of feeder speed u_1 can only reach 81.2%. Long term operation results of the proposed control system show that accidents such as the coal powder mis-emission and mill blockage can be completely avoided, the environmental pollution has been reduced and the electric energy consumption per unit coal has been
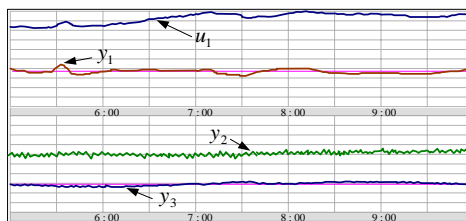

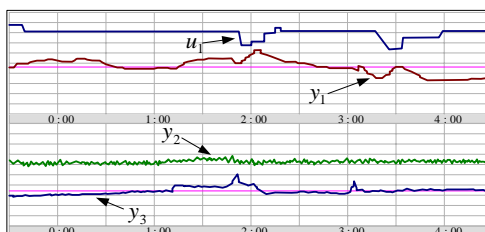Fig. 10. Actual control curves under the proposed intelligent decoupling control strategy

Fig. 11. Actual control curves under manual control

reduced by 10.3%. As a result, remarkable economic benefits have been achieved.

6. CONCLUSION

Under a suitable set of assumptions concerning the complex industrial process to be controlled, a linear model with lower order for controller design and unmodeled dynamics with higher order are used to identify complex industrial process simultaneously under certain operating point. The proposed control system uses a feedback controller and decoupling compensator to eliminate the coupling among control loops and tracking errors. Such controllers employ a feedforward compensator with a neural network to suppress the effects caused by unmodeled dynamics, where it defines a suitable switching law to switch between the controllers on different operating points of industrial processes. The simulation result and the successful real application of the control system in 200MW power units show that the developed control system is powerful in dealing with the decoupling control for complex industrial processes.

REFERENCES

Chen. L.J. and K.S. Narendra (2001). Nonlinear adaptive control using neural networks and multiple models. *Automatica*. **37**. pp.1245–1255.

Funahashi, K. (1989). On the approximate realization of continuous mappings by neural networks. *Neural Networks*, **2**, pp. 183-192.

Lang, S.J., X.Y. Gu and T.Y. Chai (1986). A multivariable generalized self-tuning controller with decoupling design. *IEEE Transactions on Automatic Control*, **31**, pp.474–477.

Shinskey, F.G. (1979). *Process Control Systems, Second Edition*. McGraw-Hill Book Company.

Tao, W.H., T.Y. Chai and H. Yue (2004). Research of dynamic mathematical model and simulation of ball coal mill system. *Journal of System Simulation*, **16**, pp. 778–780 (in Chinese).

Wittenmark, B., R. Middleton and G. Goodwin (1987). Adaptive Decoupling of Multivariable Systems. *International Journal of Control*, **46**, pp.1993–2009.

Wu L.M. and T.Y. Chai (1995). Decoupling of a class of nonlinear discrete time systems using neural networks. In: *Proceedings of the 1995 American Control Conference*, **6**, pp. 4275-4279.

Zhu, K.Y., X.F. Qin and T.Y. Chai (1999). A new decoupling design of self-tuning multivariable generalized predictive control. *International Journal of Adaptive Control*, **13**, pp.183–196.